PHYSICAL REVIEW B **100**, 201106(R) (2019)

Rapid Communications

Electronic structure of rare-earth infinite-layer $R\mathrm{NiO}_2$ (R = La, Nd)

Peiheng Jiang,[1,*] Liang Si,[1,2,*] Zhaoliang Liao,[3] and Zhicheng Zhong[1,4,†]
[1] *Key Laboratory of Magnetic Materials and Devices and Zhejiang Province Key Laboratory of Magnetic Materials and Application Technology, Ningbo Institute of Materials Technology and Engineering, Chinese Academy of Sciences, Ningbo 315201, People's Republic of China*
[2] *Institut für Festkörperphysik, TU Wien, Wiedner Hauptstraße 8-10, 1040 Vienna, Austria*
[3] *National Synchrotron Radiation Laboratory, University of Science and Technology of China, Hefei 230026, People's Republic of China*
[4] *China Center of Materials Science and Optoelectronics Engineering, University of Chinese Academy of Sciences, Beijing 100049, People's Republic of China*

(Received 30 September 2019; published 22 November 2019)

The discovery of infinite-layer nickelate superconductor marks the new era in the field of superconductivity. In the rare-earth (R) nickelates RNiO_2, although the Ni is also of d^9 electronic configuration, analogous to Cu d^9 in cuprates, whether electronic structures in infinite-layer nickelate are the same as cuprate and possess the single-band feature as well are still open questions. To illustrate the electronic structure of rare-earth infinite-layer nickelate, we perform first-principles calculations of LaNiO_2 and NdNiO_2 compounds and compare them with that of CaCuO_2 using the hybrid functional method together with Wannier projection and group symmetry analysis. Our results indicate that the Ni $d_{x^2-y^2}$ in the LaNiO_2 has weak hybridization with other orbitals and exhibits the characteristic single-band feature, whereas in NdNiO_2, the Nd f orbital hybridizes with Ni $d_{x^2-y^2}$ and is a non-negligible ingredient for transport and even high-temperature superconductivity. Given that the Cu $d_{x^2-y^2}$ in cuprate strongly hybridizes with O $2p$, the calculated band structures of nickelate imply some new band characters, which is worthy of more attention.

DOI: 10.1103/PhysRevB.100.201106

Since the discovery of high-T_C cuprate superconductors in 1986 [1], searching for new high-T_C superconductors and revealing the mechanism of high-T_C superconductivity (HTSC) are invariably at the forefront of research of condensed matter physics. Although the mechanism of HTSC in the cuprates remains a puzzle, there is a general consensus that the key structural unit, the CuO_2 plane, which exhibits characteristic quasi-two-dimensional (2D) physics of the $d_{x^2-y^2}$ orbital, plays a central role in HTSC. The Cu in cuprate has a d^9 electron configuration and the crystal field of the CuO_2 plane strongly lifts the degeneracy of the e_g orbital with $d_{x^2-y^2}$ located above d_{z^2}. The $d_{x^2-y^2}$ hybridizes with oxygen $2p$ bands, forming an effective singlet band with zero spin moment known as the Zhang-Rice singlet [2]. The hole in the oxygen site couples antiferromagnetically with the hole on the copper site. The hole doping can suppress the antiferromagnetic ordering and drive the cuprate into a superconductive phase wherein the Cooper pairs are proposed to be mediated by antiferromagnetic spin fluctuation [3,4].

Designing and fabricating an analog of a cuprate superconductor is one of the key steps towards identifying the key ingredients and unraveling the mechanism of HTSC. Nickelates are one of the ideal systems to mimic cuprates. In a bulk perovskite $R\mathrm{NiO}_3$ system, the Ni is of d^7 configuration with one electron in the doubly degenerate e_g orbitals. One idea to generate a cupratelike electronic structure is to remove the degeneracy of e_g orbitals and deplete the d_{z^2} orbital, which leads to a half-filled $d_{x^2-y^2}$ band similar to the parent compound of cuprates. This is the idea behind the theoretical proposal of $\mathrm{LaAlO}_3/\mathrm{LaNiO}_3$ heterostructures by Chaloupka and Khaliullin in 2008 [5]. The actual orbital polarization obtained by experimental efforts, however, is too small to produce a characteristic $d_{x^2-y^2}$ single-band electronic structure [6–8].

To remove the apical oxygen in nickelates and then flip the orbital configuration to lift up the $d_{x^2-y^2}$ against the d_{z^2} is another path to mimic orbital configuration in cuprates [9–15]. In this case, to half-fill the highest-energy $d_{x^2-y^2}$ orbital, Ni needs to be d^9. One promising candidate is the infinite-layer RNiO_2, which can be obtained by reducing the $R\mathrm{NiO}_3$. In infinite-layer RNiO_2, the Ni^{1+} possesses d^9 configuration with half-filled $d_{x^2-y^2}$. Exploring the superconductivity in RNiO_2 starts earlier from 2009 in $(\mathrm{La,Sr})\mathrm{NiO}_2$ [16], but no evidence of superconductivity in $(\mathrm{La,Sr})\mathrm{NiO}_2$ is found experimentally. A breakthrough is made by Li *et al.* who discovered the superconductivity in $\mathrm{Nd}_{0.8}\mathrm{Sr}_{0.2}\mathrm{NiO}_2$ with T_C ranging from 9 to 15 K depending on the samples [15]. The discovery of superconducting $\mathrm{Nd}_{0.8}\mathrm{Sr}_{0.2}\mathrm{NiO}_2$ sheds light on the era of nickelate superconductivity, and is now motivating worldwide efforts to explore this new system [17–29]. A systematic comparison between infinite-layer nickelate with cuprate can pave the way to identify essential features for superconductivity and to narrow down the range of a possible theory of HTSC. At first glance when comparing the nickelate with the cuprate, the following questions arise: What is the

---

[*] These authors contributed equally to this work.

[†] Corresponding author: zhong@nimte.ac.cn

difference of their electronic structures? Is the Zhang-Rice singlet band model still valid for nickelate? Additionally, to what extent do the *d* and *f* orbitals of the rare earth—which are close to the Fermi level—affect the electronic structure and participate in the superconductivity?

With these questions in mind, we perform first-principles density functional theory (DFT) calculations using hybrid functionals which incorporate 25% short-range Hartree-Fock exchange, 75% full-range Perdew-Burke-Ernzerhof (PBE) exchange, and 100% PBE correlation [30]. The hybrid functional performs exceptionally well in predicting the band gap of semiconductors such as Si and $SrTiO_3$, and describing systems with a mixture of itinerant and localized electrons from different orbitals, where the delicate balance between itinerancy and localization can produce multiple competing ground states and phases [31]. For the rare-earth oxides of $LaNiO_2$ and $NdNiO_2$, both the transition metal *d* electrons and lanthanide *f* electrons participate in electronic band structure near Fermi level [12,13]. The hybrid functional, which can deal with both itinerant and localized electrons without any adjustable parameters, is a very effective method to describe the electron behavior of such materials [32–35]. By performing the first-principles DFT calculation and group symmetry analysis, we show that the Ni $d_{x^2-y^2}$ in the $LaNiO_2$ has very weak hybridization with other orbitals and exhibits a characteristic single-band feature, whereas in $NdNiO_2$ the Nd *f* orbital hybridizes with Ni $d_{x^2-y^2}$ and makes the $NdNiO_2$ different from both $LaNiO_2$ and cuprates. These facts imply that a single-band model may not capture all the key ingredients of $NdNiO_2$.

We performed the DFT calculations within the generalized gradient approximation [36] and the projector augmented wave method as implemented in the Vienna *ab initio* simulation package (VASP) [37,38]. To avoid artificial results from different DFT codes, the main calculations have been checked by the WIEN2K code [39] with plane wave method and full potential. For La and Nd, 10 and 14 valence electrons of $5s^26p^65d6s^2$ and $5s^26p^64f^45d6s^2$ were considered in calculations, respectively. We performed spin-polarized calculations for $NdNiO_2$, while complex spin order is not considered for simplicity [40]. The PBEsol functional was adopted for structure relaxation. The relaxed lattice constants are $a = b = 3.88$ Å and $c = 3.35$ Å for $LaNiO_2$, $a = b = 3.86$ Å and $c = 3.24$ Å for $NdNiO_2$. A hybrid density functional of Heyd-Scuseria-Ernzerhof (HSE06) [30], which includes the short-range exact exchange function and thus can deal with both itinerant and localized electrons, was used for an accurate prediction of electronic band structure. The Brillouin zone was sampled with $12 \times 12 \times 12$ and $8 \times 8 \times 8\,k$ mesh for DFT and HSE calculations, respectively. The kinetic energy cutoff was set to 500 eV. To obtain the tight-binding model Hamiltonian, the La 5*d* and Ni 3*d* HSE bands are projected onto maximally localized Wannier functions using WIEN2WANNIER [41] and VASP2WANNIER interfaces.

The infinite-layer $RNiO_2$ is isostructural to $CaCuO_2$, which can be derived from removing the apical oxygen of the octahedra in $RNiO_3$. In detail, it is stacked by rare-earth layers and NiO_2 planes alternately in a tetragonal lattice. The rare-earth atom is surrounded by an oxygen tetragon, and the Ni atom is surrounded by a rare-earth tetragon and also by oxygen square in the NiO_2 plane. The local point group is D_{4h}, D_{4h}, and D_{2h} for La (Nd), Ni, and O, respectively. With this lattice structure, we first investigate the orbital projected electronic band structure of $LaNiO_2$ where the La *f* orbital can be neglected and only the La *d* orbital has to be considered. As shown in Fig. 1(a), six bands within the energy range of −10 to −5 eV are contributed by O *p* orbitals, and four bands of Ni t_{2g} and d_{z^2} orbitals are located at a higher range of −5 to −2 eV. Near the Fermi level between −2 and 3 eV, the bands are mainly contributed by Ni $d_{x^2-y^2}$, La d_{xy}, and La d_{z^2} orbitals. Other La *d* orbitals and all La *f* orbitals form the upper bands.

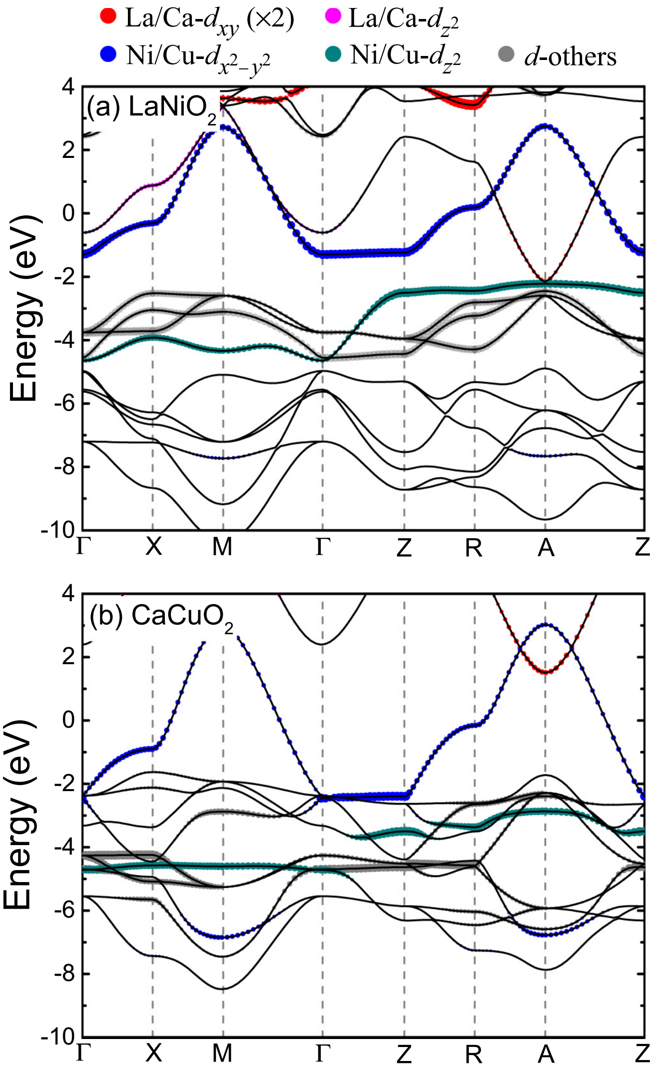

FIG. 1. Orbital projected electronic band structures of $LaNiO_2$ and $CaCuO_2$. The size of the red, magenta, blue, dark-cyan, and gray dots represents the weight of La/Ca d_{xy}, La/Ca d_{z^2}, Ni/Cu $d_{x^2-y^2}$, Ni/Cu d_{z^2}, and other *d* orbitals, respectively. The weight of La/Ca d_{xy} has been enlarged twice. The six bands within the energy range of −10 to −5 eV in $LaNiO_2$ without a label of orbital projection are contributed by O *p* orbitals, while the corresponding bands in $CaCuO_2$ within the energy range of −9 to −4 eV are contributed by both O *p* and Ni *d* orbitals. The HSE functional was used in the calculation.

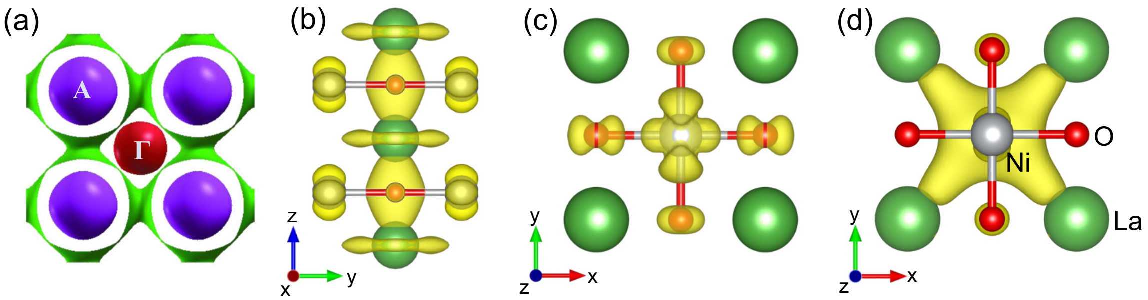

FIG. 2. (a) Fermi surface of LaNiO$_2$. Three different electron pockets around the Γ, Z, and A points are shown by red, purple, and green spheres, respectively. (b)–(d) The charge density of these three electron pockets near Fermi level.

The prominent band and orbital characters of LaNiO$_2$ can be further characterized by the Fermi surface and partial charge density. As shown in Fig. 2(a), there are two Fermi spheres around the Γ and A points with 0.10 and 0.19 electrons included, respectively, and one large electron pocket around the Γ-Z direction, which are contributed by La d_{z^2}, La d_{xy}, and Ni $d_{x^2-y^2}$ orbitals, respectively. In particular, the cylindrical distribution of the Fermi surface and the energy dispersion of the Ni $d_{x^2-y^2}$ orbital indicate a quasi-2D character along the Γ-Z direction. Figures 2(b)–2(d) display the charge density of the pockets around the Γ, Z, and A points, respectively. These localized charge distributions around the Z point and the large orbital weight of the Ni $d_{x^2-y^2}$ band together indicate the localization of this orbital. For the other pocket around the A point, the charge disperses to almost the whole space of the La atomic plane, which results from the itinerant La d_{xy} orbital. Such a nonlocalized character is consistent with the smaller orbital weight as shown in Fig. 1(a).

The orbital hybridizations are essential properties to estimate electronic structures and to investigate the single-band picture. Although the Ni $d_{x^2-y^2}$, La d_{xy}, and La d_{z^2} orbitals are all located near the Fermi level, the weak hybridization between Ni $d_{x^2-y^2}$ and other orbitals as revealed by our Wannier projection tight-binding calculation and group symmetry analysis demonstrate that the LaNiO$_2$ can be well described by a single-band picture as discussed in the following. The hybridization between two orbitals is mainly determined by two parameters. One is the energy splitting of two orbitals Δ. The other parameter is the hopping term t, which is related to orbital shape and lattice symmetry. The strength of hybridization is expressed by the formula $\sqrt{1+(\frac{2t}{\Delta})^2}-1$. A small Δ and a large t will lead to strong hybridization. In the case of weak hybridization, the system can be simplified as a single band. When the hybridization becomes strong, extra treatment of the band and theoretic model should be considered. A typical example is the modified effective single-band model, such as the Zhang-Rice singlet [2], which mixes the effective information of the p orbital into the d orbital. Another example is the Emery model [42,43], which is a three-band Hubbard model with one Cu $d_{x^2-y^2}$ and two O p orbitals.

With respect to LaNiO$_2$, our calculations show that the Ni $d_{x^2-y^2}$ has negligible hybridization with O p orbitals, which is in strong contrast to the case in cuprates. Using the CaCuO$_2$ as an example, the Cu $d_{x^2-y^2}$ orbital has strong hybridization with the O p orbital owing to small Δ and a large hopping term t. In this situation, the system is generally described by an effective d-p hybrid single-band model. While in LaNiO$_2$, the energy splitting Δ between Ni $d_{x^2-y^2}$ and O p orbitals is as big as 6 eV. Meanwhile, the orbital weight of $d_{x^2-y^2}$ in LaNiO$_2$ is much larger than CaCuO$_2$, e.g., 36% larger at the A point. Both of these facts reveal a much weaker orbital hybridization in LaNiO$_2$ than that in CaCuO$_2$. As a consequence, the d-p singlet model is not necessary for LaNiO$_2$. What is more, the Ni $d_{x^2-y^2}$ orbital is also found to not hybridize with other Ni d orbitals. First, the Ni $d_{x^2-y^2}$ and Ni t_{2g} hybridization is prohibited by orbital orthogonality as revealed by the zero hopping term between Ni $d_{x^2-y^2}$ and Ni t_{2g} (see Supplemental Material [44]). Secondly, the interorbital hybridization between Ni $d_{x^2-y^2}$ and the Ni d_{z^2} is energetically unfavorable due to large energy splitting Δ in spite of the nonzero hopping term t of 0.035 eV between Ni $d_{x^2-y^2}$ and Ni d_{z^2}.

Our results also indicate weak hybridization between the Ni $d_{x^2-y^2}$ and the La d orbital. The hopping terms from the Ni $d_{x^2-y^2}$ to La d_{xy/z^2} orbitals are zero due to the orbital orthogonality [44]. Moreover, when the wave vector approaches $k_x = 0.5$ (Γ-X path), the wave vector group is reduced from $D_{4h}(\Gamma)$ to $C_{2v}(\Gamma\text{-}X)$ and the Ni $d_{x^2-y^2}$ band is described by A_1, which is the same with the La d_{z^2} band. The hybridization between Ni $d_{x^2-y^2}$ and La d_{z^2} is allowed in terms of their same symmetry. Yet, a large Δ between Ni $d_{x^2-y^2}$ and La d_{z^2} severely reduces hybridization. Along the X-M-Γ path, the Ni $d_{x^2-y^2}$ band is described by $B_1(C_{2v})$ while the La d_{z^2} band is described by A_1 (C_{2v}); the hybridization is prohibited by the difference in symmetry. When these two orbitals approach the A point ($k_x = k_y = k_z = 0.5$), the characters and symmetric properties of the bands do not change: the Ni $d_{x^2-y^2}$ band hosts a representation of $A_2(C_{2v})$ and the La d_{xy} band is described by $B_1(C_{2v})$. The most striking consequence of the weak/no hybridization of Ni $d_{x^2-y^2}$ with other orbitals is that no hybridization gap (band anticrossing) is formed in the whole Brillouin zone near Fermi level. Further analysis indicates that at the $k_z = 0.5$ plane a nodal line is formed and protected by crystal symmetry. The corresponding symmetry analysis can be found in the Supplemental Material [44]. With quasi-single-band behavior of Ni $d_{x^2-y^2}$, a tight-binding Hamiltonian is constructed through Wannier projection [44].

By replacing La with Nd, the partially filled f electrons are introduced into the system. Figure 3 shows the orbital

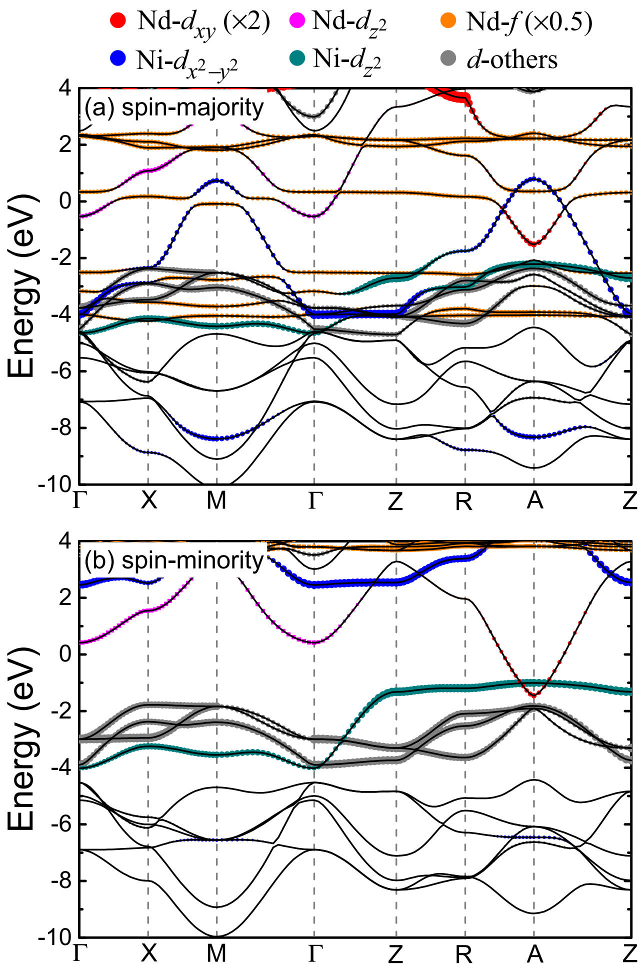

FIG. 3. Orbital projected electronic band structure of NdNiO$_2$. The size of the red, magenta, blue, orange, dark-cyan, and gray dots represents the weight of Nd d_{xy}, Nd d_{z^2}, Nd f, Ni $d_{x^2-y^2}$, Ni d_{z^2}. and other d orbitals, respectively. The weight of the Nd d_{xy} and Nd f orbitals has been enlarged twice and half time, respectively. The HSE functional and spin polarization were considered in the calculation.

projected electronic band structure of NdNiO$_2$. Here the spin polarization is considered because of the large local magnetic moment of Nd f electrons. The total magnetic moment is 3.91μ_B per unit cell, and the local moments of Nd f and Ni d are 3.03μ_B and 0.89μ_B, respectively. As shown in Fig. 3, there is a large splitting between the spin majority and minority channels of the Ni $d_{x^2-y^2}$ orbital. The Nd d orbitals still cross Fermi level and self-dope the system like La d orbitals in LaNiO$_2$. We now focus on the spin majority channel and find that the Nd f orbitals are much more localized and almost do not disperse. Three f bands below Fermi level and one f band cross Fermi level, contributing a local moment of 3.03 μ_B. Since f electrons are located near Fermi level, a d-f hybridization occurs at the M point. This hybridization is so strong that the d orbital is split and a gap is opened. In contrast, such hybridization does not occur at the A point. Unlike the quasi-single-band behavior in LaNiO$_2$ and CaCuO$_2$, the band dispersion of NdNiO$_2$ near Fermi energy exhibits an unusual behavior: the dominating Ni $d_{x^2-y^2}$ band shows strong hybridization with f orbitals around the M point, whereas it exhibits quasi-single-band behavior around the A point. These characters make the electronic structures of NdNiO$_2$ differ strongly from LaNiO$_2$. The physical origin of this unusual phenomenon is explained by our symmetry analysis (for details please see Fig. S6 [44]). We can draw a conclusion that there is strong hybridization between the f and d electrons in NdNiO$_2$.

In summary, we have performed the DFT calculations of infinite-layer RNiO$_2$ (R = La, Nd) with the hybrid functional method and group symmetry analysis. Our results suggest that the Ni $d_{x^2-y^2}$ subband in LaNiO$_2$ can be treated as an isolated single band due to its weak/no hybridization with other orbitals. As a consequence, the 2D single-band character in LaNiO$_2$ becomes even stronger than that of CaCuO$_2$. Meanwhile, the La d electrons have two non-negligible impacts. One is the self-doping effect, which might lead to the redistribution of charge and alter the magnetic properties of the system. The second effect is that the interaction between La d electrons and Ni d electrons might be substantial. The itinerant La-d orbitals provide an electron background in LaNiO$_2$, while the 2D single band of the Ni $d_{x^2-y^2}$ orbital is localized with the energy near Fermi level, and only weak hybridization exists between them.

For NdNiO$_2$, the Nd d orbital behaves similarly to the La d orbital in LaNiO$_2$. The Nd d orbital also crosses Fermi level and has a self-doping effect. The hybridization between the Nd d orbital and Ni $d_{x^2-y^2}$ is also very weak. The big difference between NdNiO$_2$ and LaNiO$_2$ arises from their f orbital. Different from the LaNiO$_2$ wherein the f orbitals are far from Fermi level and Ni d orbitals, the Nd f orbitals are located near Fermi level and strongly hybridize with Ni $d_{x^2-y^2}$ in NdNiO$_2$. Additionally, the large magnetic moment of Nd f orbitals can lead to spin polarization of the Ni orbital and would affect the magnetic ordering of NdNiO$_2$. The magnetization of f electrons would also make the single Ni $d_{x^2-y^2}$ model not as effective as that in LaNiO$_2$. The role of the rare-earth f orbital in affecting the electronic structure then suggests a new twist of freedom to engineer superconductive and magnetic behavior in infinite-layer nickelates by engineering the $f-d$ orbital hybridization, which is usually not feasible in cuprates.

We thank Dr. Yi Lu at University of Heidelberg and Dr. Lei Li at Northwestern Polytechnical University for valuable discussions. We gratefully acknowledge financial support from the National Key R&D Program of China (Grant No. 2017YFA0303602), the National Nature Science Foundation of China (Grants No. 11774360, No. 11904373, and No. 51931011), and 3315 Program of Ningbo. L.S. was also supported by the European Research Council (ERC) under the European Union's Seventh Framework Program (FP/2007-2013) through ERC Grant No. 306447, and by the Austrian Science Fund (FWF) through project P 30997. Research by Z.L. was financially supported by Hundred Talent Program of the Chinese Academy of Sciences, the Fundamental Research Funds for the Central Universities and National Nature Science Foundation of China (Grants No. 11974325). Calculations were performed at the Supercomputing Center of Ningbo Institute of Materials Technology and Engineering.

[1] J. G. Bednorz and K. A. Muller, Z. Phys. B **64**, 189 (1986).

[2] F. C. Zhang and T. M. Rice, Phys. Rev. B **37**, 3759 (1988).

[3] P. W. Anderson, Phys. Rev. Lett. **96**, 017001 (2006).

[4] P. W. Andersen, Science **235**, 1196 (1987).

[5] J. Chaloupka and G. Khaliullin, Phys. Rev. Lett. **100**, 016404 (2008).

[6] E. Detemple, Q. M. Ramasse, W. Sigle, G. Cristiani, H. U. Habermeier, E. Benckiser, A. V. Boris, A. Frano, P. Wochner, M. Wu, B. Keimer, and P. A. van Aken, Appl. Phys. Lett. **99**, 211903 (2011).

[7] P. Hansmann, X. Yang, A. Toschi, G. Khaliullin, O. K. Andersen, and K. Held, Phys. Rev. Lett. **103**, 016401 (2009).

[8] Z. Zhong, P. X. Xu, and P. J. Kelly, Phys. Rev. B **82**, 165127 (2010).

[9] M. Hepting, R. J. Green, Z. Zhong, M. Bluschke, Y. E. Suyolcu, S. Macke, A. Frano, S. Catalano, M. Gibert, R. Sutarto, F. He, G. Cristiani, G. Logvenov, Y. Wang, P. A. van Aken, P. Hansmann, M. Le Tacon, J. M. Triscone, G. A. Sawatzky, B. Keimer, and E. Benckiser, Nat. Phys. **14**, 1097 (2018).

[10] Z. Liao, E. Skoropata, J. W. Freeland, E. J. Guo, R. Desautels, X. Gao, C. Sohn, A. Rastogi, T. Z. Ward, T. Zou, T. Charlton, M. R. Fitzsimmons, and H. N. Lee, Nat. Commun. **10**, 589 (2019).

[11] M. A. Hayward, M. A. Green, M. J. Rosseinsky, and J. Sloan, J. Am. Chem. Soc. **121**, 8843 (1999).

[12] K. W. Lee and W. E. Pickett, Phys. Rev. B **70**, 165109 (2004).

[13] V. I. Anisimov, D. Bukhvalov, and T. M. Rice, Phys. Rev. B **59**, 7901 (1999).

[14] A. Ikeda, T. Manabe, and M. Naito, Phys. C (Amsterdam, Neth.) **495**, 134 (2013).

[15] D. Li, K. Lee, B. Y. Wang, M. Osada, S. Crossley, H. R. Lee, Y. Cui, Y. Hikita, and H. Y. Hwang, Nature (London) **572**, 624 (2019).

[16] M. Kawai, S. Inoue, M. Mizumaki, N. Kawamura, N. Ichikawa, and Y. Shimakawa, Appl. Phys. Lett. **94**, 082102 (2009).

[17] A. S. Botana and M. R. Norman, arXiv:1908.10946.

[18] H. Sakakibara, H. Usui, K. Suzuki, T. Kotani, H. Aoki, and K. Kuroki, arXiv:1909.00060.

[19] J. E. Hirscha and F. Marsiglio, Phys. C (Amsterdam, Neth.) **566**, 1353534 (2019).

[20] M. Jiang, M. Berciu, and G. A. Sawatzky, arXiv:1909.02557.

[21] M. Hepting, D. Li, C. J. Jia, H. Lu, E. Paris, Y. Tseng, X. Feng, M. Osada, E. Been, Y. Hikita, Y.-D. Chuang, Z. Hussain, K. J. Zhou, A. Nag, M. Garcia-Fernandez, M. Rossi, H. Y. Huang, D. J. Huang, Z. X. Shen, T. Schmitt, H. Y. Hwang, B. Moritz, J. Zaanen, T. P. Devereaux, and W. S. Lee, arXiv:1909.02678.

[22] X. Wu, D. D. Sante, T. Schwemmer, W. Hanke, H. Y. Hwang, S. Raghu, and R. Thomale, arXiv:1909.03015.

[23] Y. Nomura, M. Hirayama, T. Tadano, Y. Yoshimoto, K. Nakamura, and R. Arita, arXiv:1909.03942.

[24] J. Gao, Z. Wang, C. Fang, and H. Weng, arXiv:1909.04657.

[25] S. Ryee, H. Yoon, T. J. Kim, M. Y. Jeong, and M. J. Han, arXiv:1909.05824.

[26] G.-M. Zhang, Y.-F. Yang, and F.-C. Zhang, arXiv:1909.11845.

[27] N. Singh, arXiv:1909.07688.

[28] H. Zhang, L. Jin, S. Wang, B. Xi, X. Shi, F. Ye, and J.-W. Mei, arXiv:1909.07427.

[29] S. Fomichev, G. Khaliullin, and M. Berciu, arXiv:1909.06449.

[30] A. V. Krukau, O. A. Vydrov, A. F. Izmaylov, and G. E. Scuseria, J. Chem. Phys. **125**, 224106 (2006).

[31] B. G. Janesko, T. M. Henderson, and G. E. Scuseria, Phys. Chem. Chem. Phys. **11**, 443 (2009).

[32] P. J. Hay, R. L. Martin, J. Uddin, and G. E. Scuseria, J. Chem. Phys. **125**, 34712 (2006).

[33] J. L. F. Da Silva, M. V. Ganduglia-Pirovano, J. Sauer, V. Bayer, and G. Kresse, Phys. Rev. B **75**, 045121 (2007).

[34] J. Hong, A. Stroppa, J. Íñiguez, S. Picozzi, and D. Vanderbilt, Phys. Rev. B **85**, 054417 (2012).

[35] C. Franchini, J. Phys.: Condens. Matter **26**, 253202 (2014).

[36] J. P. Perdew, K. Burke, and M. Ernzerhof, Phys. Rev. Lett. **77**, 3865 (1996).

[37] G. Kresse and J. Furthmüller, Comput. Mater. Sci. **6**, 15 (1996).

[38] G. Kresse and J. Furthmüller, Phys. Rev. B **54**, 11169 (1996).

[39] P. Blaha, K. Schwarz, G. K. H. Madsen, D. Kvasnicka, J. Luitz, R. Laskowski, F. Tran, and L. D. Marks, *WIEN2k: An Augmented Plane Wave and Local Orbitals Program for Calculating Crystal Properties* (Vienna University of Technology, Austria, 2001).

[40] J. Varignon, M. Bibes, and A. Zunger, Nat. Commun. **10**, 1658 (2019).

[41] J. Kuneš, R. Arita, P. Wissgott, A. Toschi, H. Ikeda, and K. Held, Comput. Phys. Commun. **181**, 1888 (2010).

[42] V. J. Emery, Phys. Rev. Lett. **58**, 2794 (1987).

[43] V. J. Emery and G. Reiter, Phys. Rev. B **38**, 4547 (1988).

[44] See Supplemental Material at http://link.aps.org/supplemental/10.1103/PhysRevB.100.201106 for electronic band structures of LaNiO under different schemes and effects, Wannier projection, and symmetry analysis.